PRP Pharmacology Research & Perspectives
Open Access

ORIGINAL ARTICLE

Metabolism and disposition of MM-433593, a selective FAAH-1 inhibitor, in monkeys

Ali R. Banijamali[1], James D. Wakefield[1], Ara H. Mermerian[2] & Robert W. Busby[1]

[1]Analytical Pharmacology/Drug Metabolism and Pharmacokinetics, Ironwood Pharmaceuticals, Cambridge, Massachusetts
[2]Medicinal Chemistry, Ironwood Pharmaceuticals, Cambridge, Massachusetts

Keywords
Endocannabinoids, FAAH-1 inhibitor, glucuronide conjugate, hepatocyte metabolites, indole ketoamide, monkey pharmacokinetics, *N*-acetylcysteine conjugate, sulfate conjugate

Correspondence
Ali R. Banijamali, Analytical Pharmacology/Drug Metabolism and Pharmacokinetics, Ironwood Pharmaceuticals, 301 Binney Street, Cambridge, MA 02142. Tel: 617-768-2653; Fax: 617-494-0480; E-mail: abanijamali@ironwoodpharma.com

Funding Information
No funding information provided.

Received: 16 May 2014; Accepted: 27 May 2014

Pharma Res Per, 2(5), 2014, e00059, doi: 10.1002/prp2.59

doi: 10.1002/prp2.59

Abstract

MM-433593 is a highly potent and selective inhibitor of fatty acid amide hydrolase-1 (FAAH-1) with potential utility as an orally administered treatment of pain, inflammation, and other disorders. In this study, we investigated the metabolism and pharmacokinetics of MM-433593 in monkeys, and compared plasma and urine metabolites of this compound to the in vitro metabolites produced by monkey hepatocytes. Intravenous administration of MM-433593 to cynomolgus monkeys produced a rapid distribution phase and slower elimination phase with a mean systemic clearance rate of 8–11 mL/min/kg. Absolute oral bioavailability was determined to be 14–21% with maximum plasma concentrations reached ~3 h (T_{max}) following a 10 mg/kg oral dose. The average terminal half-life of MM-433593 was 17–20 h, and there were no qualitative sex differences in the metabolite profile of MM-433593. The major site of metabolism was oxidation of the methyl group at the five position of the indole ring, which was confirmed by chromatography and mass spectrometry comparison to a synthesized authentic standard. This metabolite was further oxidized to the corresponding carboxylic acid and/or conjugated with sulfate, glucuronide, or glutathione. In all, 18 metabolites were found in plasma and urine. In vitro incubations of MM-433593 with monkey hepatocytes yielded 13 metabolites, all of which were found in vivo, indicating a good correlation between the in vitro and in vivo metabolism data. A comprehensive pathway for the metabolism of MM-433593 is proposed, including a plausible, five-step biotransformation for the formation of *N*-acetylcysteine conjugate metabolite (M18) from the hydroxylated parent (M5).

Abbreviations

eCB, Endocannabinoid; CNS, central nervous system; AEA, arachidonoyl ethanolamide (anandamide); FAA, fatty acid amide; FAAH, fatty acid amide hydrolase; LEA, *N*-linoleoylethanolamine; OEA, *N*-oleoyl ethanolamide; PEA, *N*-palmitoyl ethanolamide; HPCL, high-performance liquid chromatography; UPCL, ultraperformance liquid chromatography; MRM, multiple reaction monitoring; MRT, mean residence time; AUC, area under the curve.

Introduction

Ironwood Pharmaceuticals has developed MM-433593, a novel indole ketoamide derivative, as an orally administered, small molecule inhibitor of fatty acid amide hydrolase (FAAH). MM-433593 specifically inhibits the FAAH-1 isoform with potential utility for the treatment of pain, inflammation, and other disorders modulated by the endocannabinoid (eCB) system. FAAH-1 is a serine hydrolase that is broadly expressed in the central nervous system (CNS) and the periphery and inactivates (via hydrolysis) the biologically active fatty acid amide (FAA) family of signaling lipids, which includes the eCB anandamide (AEA) (Cravatt et al. 1996; Goparaju et al. 1998).

eCBs are endogenous agonists of the cannabinoid receptor, and they have anti-inflammatory and analgesic activities (Calignano et al. 1998; Jaggar et al. 1998). Degradation of eCBs by FAAH is an important regulator of AEA levels in vivo; genetic or pharmacologic ablation of FAAH-1 activity results in elevated FAA levels in peripheral and nervous system tissues which correlate with anti-inflammatory and analgesic effects in multiple animal models (Cravatt et al. 2001, 2004; Ahn et al. 2009; Schlosburg et al. 2009; Blankman and Cravatt 2013). FAAH inhibitors have the potential to increase AEA levels and thereby act as novel therapeutics for the treatment of pain, anxiety, and neurogenerative disorders (Cravatt and Lichtman 2003; Piomelli 2003; Maccarrone 2006). Unlike some other FAAH inhibitors that have been described, MM-433593 does not covalently modify FAAH-1 at the active site and this inhibitor is >100-fold more selective for human FAAH-1 enzyme relative to human FAAH-2, the second FAAH enzyme that has been identified in primates (Wei et al. 2006). Administration of MM-433593 elevates FAAs in mice, rats, and monkeys and has both anti-inflammatory and analgesic effects in animal models of pain and inflammation (unpubl. data). In this study, the objectives were to investigate the metabolism and pharmacokinetics of MM-433593 in monkeys, the nonrodent species used in toxicology studies, to compare the metabolites identified in plasma and urine to those produced by monkey hepatocytes, and to propose a plausible pathway for formation of each metabolite.

Materials and Methods

MM-433593, internal standard MM-433593-$^{13}C_6$, and metabolite standards were synthesized at Ironwood Pharmaceuticals, Inc. (Cambridge, MA). All reagents and solvents used in the syntheses were purchased commercially (Sigma-Aldrich, St. Louis, MO; or Alfa Aesar, Ward Hill, MA) and used without any purification. Solvents of high-performance liquid chromatography (HPLC) grade were purchased from Thermo Fisher Scientific (Waltham, MA). Characterization of synthetic intermediates and final products was achieved by ^{1}H and ^{13}C NMR, and conducted on a Varian AS 400 system (Agilent Technologies, Santa Clara, CA) or a Bruker Ascend 500 system (Bruker Biospin Corporation, Billerica, MA). Quantitative mass spectrometry was conducted on SCIEX API 4000 triple quadrupole mass spectrometer (Applied Biosystems/MDS, Foster City, CA). Thermo LTQ Orbitrap Discovery™ mass spectrometer system (Thermo Scientific, San Jose, CA) coupled to a Waters Acquity™ ultraperformance liquid chromatography (UPLC) system (Waters Corporation, Milford, MA) was used for characterization of metabolites. Cryopreserved male cynomolgus monkey hepatocytes were purchased from XenoTech (Kansas City, KS).

Hepatocytes incubation

The hepatocytes (3.4×10^6 cells per assay) were incubated with 10 μmol/L MM-433593 in 1.7 mL of incubation media (Waymouth's Medium) at 37°C in a 5% CO_2 atmosphere incubator. Following a 10 min of preincubation of the cell suspension at 37°C, the reaction was started by addition of 17 μL of substrate. At 90 min, the incubation was terminated by addition of two volumes of ice-cold acetonitrile. The resulting mixtures were centrifuged to remove cellular debris. The supernatant was collected and concentrated to near dryness and then reconstituted in 100 μL of water: acetonitrile (1:1, v/v) for liquid chromatography/mass spectrometry (LC/MS) analysis.

Dosing and sample collection for pharmacokinetic evaluation

Single doses of MM-433593 were administered either orally by gavage (PO) at 10 mg/kg or intravenously (IV) as a bolus injection at 1 mg/kg to groups of six male and six female cynomolgus monkeys at MPI Research, Inc. (Mattawan, MI). The IV formulation was prepared as a 1 mg/mL solution of MM-433593 in 10% dimethylimidazolidinone, 35% propylene glycol, 15% ethanol, and 40% of 5% dextrose for injection. The PO formulation was prepared as a 1 mg/mL suspension of MM-433593 in 10% vitamin E TPGS and 0.01% simethicone in deionized water. Blood samples were collected at 0.25, 0.5, 0.75, 1, 2, 3, 4, 5, 6, 7, 8, 10, 12, 18, 24, 36, 48, 60, and 72 h after the oral dose; and 0.033 (2 min), 0.167 (10 min), 0.333 (20 min), 0.5, 0.75, 1, 2, 4, 6, 8, 10, 12, 15, 18, 24, 36, 48, 60, and 72 h after the intravenous dose, and plasma was isolated by centrifugation.

Dosing and sample collection for metabolite profile analysis

For metabolite profiling, plasma and urine samples were collected from male and female monkeys that were given five daily (QD) MM-433593 doses of 1000 mg/kg PO. Blood samples were taken at 2, 4, 8, 12, and 24 h post dose and urine was collected up to 24 h post dose on day 5.

Preparation of plasma samples for pharmacokinetic evaluation

Sample extracts were prepared by protein precipitation of 50-μL aliquots with eight volumes of acetonitrile in the presence of MM-433593-$^{13}C_6$ internal standard, evaporated to dryness in a TurboVap (Zymark, Hopkinton, MA), reconstituted with 200 μL of water-acetonitrile

(70:30), and MM-433593 concentrations were measured using LC/MS.

Preparation of plasma and urine samples for metabolite profile analysis

Plasma samples were thawed on ice prior to extraction. Aliquots (100 μL) from male and female monkeys were pooled, separately, and mixed with three volumes of ice-cold acetonitrile, mixed vigorously by vortexing, and stored on ice for ~1 h to enhance the protein precipitation. After vortexing once more, the precipitated samples were centrifuged at 16,000*g* for 10 min at room temperature. The supernatant was transferred to fresh tubes and solvent was evaporated under nitrogen at 45°C in a TurboVap. The dried samples were reconstituted with 100 μL of 50:50 (v/v) 0.1% formic acid in water: 0.1% formic acid in 95:5 acetonitrile: water, vortexed and transferred into LC/MS vials.

The urine collected up to 24 h post-dose from male and female monkey was used for metabolite identification. Urine aliquots (0.5 mL) were transferred into microcentrifuge tubes. After adding 1 mL of ice-cold acetonitrile, each tube was mixed vigorously by vortexing and stored on ice for about 1 h. The precipitated samples were centrifuged at 16,000*g* for 10 min at room temperature. The supernatant was transferred to fresh tubes and solvent was evaporated under nitrogen at 45°C in a TurboVap. The dried samples were reconstituted with 100 μL of 50:50 (v/v) 0.1% formic acid in water: 0.1% formic acid in 95:5 acetonitrile: water, vortexed and transferred to LC/MS vials.

Quantitative LC/MS analysis

Sample extracts were analyzed using an Applied Biosystems/MDS SCIEX API 4000 triple quadrupole mass spectrometer equipped with an Agilent 1200 HPLC. The mass spectrometer was operated in multiple reaction monitoring (MRM) mode, with resolution set to 0.7 Da for isolating the 448.1 → 151.0 transition. Calibration curves were created using a 1/x-weighted linear regression of analyte concentration versus instrument response ratio (ratio of analyte peak area to internal standard peak area).

Qualitative LC/MS analysis

All LC/MS analyses were carried out under the conditions summarized in Table 1. Chromatographic separation of MM-433593 and its metabolites was conducted using a Hypersil Gold C18 analytical column (Thermo Electron, Bellefonte, PA). ESI^+ LC/MS and product ion mass spectrometry (MS^2), in combination with high-resolution accurate mass spectrometry, were used for structural elucidation of metabolites. The mass spectrometer was operated in positive electrospray ionization (ESI^+) mode. A scan range of 100–1000 *m/z* was used to detect the test article and its metabolites in the samples. Use of positive electrospray ionization resulted in the formation of protonated adducts of the protonated molecule $[M+H]^+$ peaks. LC/MS^2 was then conducted to obtain fragmentation ions of the $[M+H]^+$ peaks.

Pharmacokinetic data analysis

The plasma concentration data were summarized statistically and noncompartmental analysis was performed using WinNonlin version 5.2 (Pharsight, Mountain View, CA) to determine the following pharmacokinetic parameters for MM-433593: maximum observed plasma concentration (C_{max}), first time to C_{max} (T_{max}), extrapolated initial plasma concentrations (C_0) and apparent volume of the central compartment (V_c) following intravenous administration, terminal phase half-life ($t_{1/2}$), mean residence time (MRT), area under the concentration–time curve from time zero to the time of the last sample collected (AUC_{all}), exposure extrapolated to infinity (AUC_{inf}), systemic clearance (CL), steady-state volume of distribution (Vd_{ss}), terminal phase volume of distribution (Vd_z), apparent clearance following oral dosing (CL/F), and absolute oral bioavailability (F).

Synthesis

1-(4-chlorobenzyl)-3-(2-(2-methoxypyridin-4-ylamino)-2-oxoacetyl)-2-methyl-1H-indole-5-carboxylic acid (M9)

To a solution of 2-methyl-1H-indole-5-carbonitrile A (417 mg, 2.67 mmol) and 1-chloro-4-(chloromethyl)benzene (0.337 ml, 2.67 mmol) in dimethylsulfoxide (8 mL) at room temperature was added powdered potassium hydroxide (300 mg, 5.34 mmol). The reaction was stirred at room temperature for 12 h, after which the reaction was diluted in water, extracted with dichloromethane (3 × 50 mL), dried (sodium sulfate), filtered, and concentrated to a clear residue. Purification was achieved by silica gel chromatography to afford 1-(4-chlorobenzyl)-2-methyl-1H-indole-5-carbonitrile (600 mg, 2.14 mmol, 80% yield) as an off-white solid.

To a slurry of 1-(4-chlorobenzyl)-2-methyl-1H-indole-5-carbonitrile (566 mg, 2.02 mmol) in absolute ethanol (5 mL) was added an aqueous 3 mol/L solution of sodium hydroxide (3.36 mL, 10.1 mmol). The reaction mixture was heated in the microwave at 170°C for 15 min after which the reaction mixture was diluted in

Table 1. MM-433593 HPLC and mass spectrometry conditions.

MASS spectrometer	Thermo Scientific LTQ Orbitrap Discovery™		
Ion mode	Positive ion electrospray (ESI^+)		
Analyzer	Hybrid linear ion trap/orbitrap		
Mass range	Normal		
Resolution	30,000		
Scan type	Full		
Data type	Centroid		
Scan range	100–1000 *m/z*		
Electrospray voltage	5 kV		
Sheath gas	60		
Auxiliary gas	20		
Sweep gas	0.6		
Ion transfer tube temp.	300°C		
HPLC	Waters acquity UPLC		
UV	Waters acquity PDA detector (λ = 250–325 nm)		
Column	Thermo hypersil gold, 2.1 × 50 mm, 1.9 μm		
Flow rate	500 μL/min		
Column temperature	40°C		
Autosampler temperature	4°C		
Injection volume	20 μL		
Mobile phase	A = 0.05% acetic acid in 95:5 (v/v) water: acetonitrile		
	B = 0.05% acetic acid in 95:5 (v/v) acetonitrile: water		
Gradient	Time (min)	% A	% B
	0	95	5
	2.0	95	5
	17.0	20	80
	18.0	20	80
	19.0	95	5

ESI^+, positive electrospray ionization; HPLC, high-performance liquid chromatography; UPLC, ultraperformance liquid chromatography; PDA, photodiode array.

water, then washed with ethyl acetate (3 × 50 mL). The aqueous layer was acidified with aqueous 3 mol/L hydrochloric acid solution, then back extracted with ethyl acetate (3 × 50 mL), dried (sodium sulfate), filtered, and concentrated to afford 1-(4-chlorobenzyl)-2-methyl-1H-indole-5-carboxylic acid B (350 mg, 1.17 mmol, 58% yield) as a tan solid.

To a slurry of 1-(4-chlorobenzyl)-2-methyl-1H-indole-5-carboxylic acid 6 (350 mg, 1.17 mmol) in diethyl ether (50 mL) and methanol (50 mL) was added a 2 mol/L solution in diethyl ether of trimethylsilyldiazomethane (2.92 mL, 5.84 mmol). The reaction was stirred at room temperature for 30 min, after which the reaction mixture was concentrated to afford the product, methyl 1-(4-chlorobenzyl)-2-methyl-1H-indole-5-carboxylate (350 mg, 1.12 mmol, 96% yield) as a tan solid, which was used in the subsequent step without any purification.

To a −10°C solution of methyl 1-(4-chlorobenzyl)-2-methyl-1H-indole-5-carboxylate (56.2 mg, 0.179 mmol) in dichloromethane (10 mL) was added neat oxalyl chloride (0.0170 mL, 0.192 mmol). The reaction was stirred at −10°C for 30 min, after which another equivalent of oxalyl chloride (0.0170 mL, 0.192 mmol) was added, and the reaction was continued by stirring at −10°C. After 50 min, the solvent was evacuated and the reaction was concentrated to dryness, then reconstituted in dichloromethane (10 mL), and cooled to −10°C. To this solution was added 2-methoxypyridin-4-amine (22.9 mg, 0.184 mmol), followed by triethylamine (0.0500 mL, 0.358 mmol). The reaction mixture was stirred at −10°C, then slowly warmed to room temperature. After 30 min, the reaction was diluted with water, extracted with dichloromethane (3 × 30 mL), dried (sodium sulfate), filtered, and concentrated to afford a gold solid. Purification was achieved by silica gel chromatography to afford methyl 1-(4-chlorobenzyl)-3-(2-(2-methoxypyridin-4-ylamino)-2-oxoacetyl)-2-methyl-1H-indole-5-carboxylate (50.6 mg, 0.101 mmol, 56% yield) as a white solid.

To a solution of 1-(4-chlorobenzyl)-3-(2-(2-methoxypyridin-4-ylamino)-2-oxoacetyl)-2-methyl-1H-indole-5-carboxylate (46.8 mg, 0.0950 mmol) in tetrahydrofuran (3 mL) and water (3 mL) was added a 1 mol/L solution of aqueous sodium hydroxide (0.285 mL, 0.285 mmol). The reaction mixture was stirred at room temperature for

30 min, after which additional 1 mol/L solution of aqueous sodium hydroxide (0.285 mL, 0.285 mmol) was added. After stirring at room temperature for 30 min, the reaction mixture was heated to 60°C for 20 min, then dropped to 40°C, and stirred at this temperature for 14 h. After cooling to room temperature, the tetrahydrofuran was removed, and the resulting residue was diluted in water, neutralized by the addition of aqueous 6 mol/L hydrochloric acid solution (95 μL), extracted with ethyl acetate (3 × 30 mL), dried (sodium sulfate), filtered, and concentrated to afford a residue which was purified on silica gel to provide 1-(4-chlorobenzyl)-3-(2-(2-methoxypyridin-4-ylamino)-2-oxoacetyl)-2-methyl-1H-indole-5-carboxylic acid M9 (19.7 mg, 0.0410 mmol, 43% yield) as a gold solid. ^{1}H NMR (400 MHz, CD_3OD) δ (ppm): 8.79 (s, 1H), 8.06 (s, 1H), 7.93 (dd, 1H), 7.45 (d, 1H), 7.31–7.33 (m, 3H), 7.24 (dd, 1H), 7.05 (d, 2H), 5.56 (s, 2H), 3.91 (s, 3H), 2.67 (s, 3H). ^{13}C NMR (125 MHz, CD_3OD) δ (ppm): 184.7, 166.6, 165.5, 149.3, 147.6, 147.1, 138.9, 134.9, 133.3, 128.7, 127.5, 126.0, 124.7, 122.9, 110.5, 109.5, 108.4, 99.6, 52.9, 45.8, 11.5 (2 aromatic ^{13}C shifts isochronous).

2-(1-(4-chlorobenzyl)-5-(hydroxymethyl)-2-methyl-1H-indol-3-yl)-*N*-(2-methoxypyridin-4-yl)-2-oxoacetamide (M5)

To a 0°C solution of 1-(4-chlorobenzyl)-2-methyl-1H-indole-5-carboxylic acid B (515 mg, 1.72 mmol) in tetrahydrofuran (10.7 mL) was added a 1 mol/L solution of borane-tetrahydrofuran complex (3.44 mL, 3.44 mmol) drop wise over 5 min. The reaction was maintained at 0°C for 2 h, after which additional 1 mol/L solution of borane-tetrahydrofuran complex (0.5 mL) solution was added. The reaction was allowed to warm up to temperature. After 30 min, the reaction mixture was quenched by the addition of methanol (2 mL), extracted with ethyl acetate (3 × 50 mL), washed with saturated sodium bicarbonate solution (3 × 50 mL), dried (sodium sulfate), filtered, and concentrated to a clear residue which solidified to a white solid under vacuum. Purification of this material was achieved by silica gel chromatography to afford (1-(4-chlorobenzyl)-2-methyl-1H-indol-5-yl)methanol C (390 mg, 1.37 mmol, 79% yield) as a white solid.

To a 0°C solution of C (482 mg, 1.69 mmol) in dichloromethane (15 mL) was added triethylamine (0.282 mL, 2.02 mmol), followed by acetic anhydride (0.167 mL, 1.77 mmol) and 4-dimethylaminopyridine (10.3 mg, 0.0840 mmol). The reaction was stirred at 0°C for 14 h, after which it was extracted with dichloromethane (3 × 50 mL), dried (sodium sulfate), filtered, and concentrated to afford (1-(4-chlorobenzyl)-2-methyl-1H-indol-5-yl)methyl acetate (512 mg, 1.56 mmol, 93% yield) as a yellow oil. This material was used in the next step without further purification.

The synthesis of the corresponding ketoamide of C (see Scheme 1) was achieved using the same procedure used in the synthesis of metabolite M9. The product (1-(4-chlorobenzyl)-3-(2-(2-methoxypyridin-4-ylamino)-2-oxoacetyl)-2-methyl-1H-indol-5-yl)methyl acetate (176 mg, 0.348 mmol, 67% yield) was isolated as an off-white solid.

To a 0°C solution of (1-(4-chlorobenzyl)-3-(2-(2-methoxypyridin-4-ylamino)-2-oxoacetyl)-2-methyl-1H-indol-5-yl)methyl acetate (173 mg, 0.342 mmol) in tetrahydrofuran (3.4 mL) and water (3.4 mL) was added an aqueous 3 mol/L solution of sodium hydroxide (342 μL, 1.03 mmol). After 2 h, the reaction was warmed to room temperature, after which additional 3 mol/L sodium hydroxide solution was added (114 μL, 0.343 mmol). The reaction was stirred for an additional 30 min at room temperature, after which the mixture was concentrated, diluted in water, quenched by the addition of 6 mol/L hydrochloric acid solution (230 μL), extracted with ethyl acetate (3 × 50 mL), dried (sodium sulfate), filtered, and concentrated to a solid. Purification by silica gel chromatography afforded 2-(1-(4-chlorobenzyl)-5-(hydroxymethyl)-2-methyl-1H-indol-3-yl)-*N*-(2-methoxypyridin-4-yl)-2-oxoacetamide M5 (121 mg, 0.257 mmol, 75% yield) as a pale yellow solid. ^{1}H NMR (400 MHz, CD_3OD) δ (ppm): 8.04–8.07 (m, 2H), 7.42 (d, 1H), 7.22–7.32 (m, 5H), 7.04 (d, 2H), 5.53 (d, 2H), 4.88 (s, 2H), 3.92 (s, 3H), 2.67 (s, 3H). ^{13}C NMR (125 MHz, $CDCl_3$) δ (ppm): 183.5, 161.4, 161.9, 148.9, 147.7, 146.1, 136.2, 136.0, 133.9, 133.7, 129.3, 127.3, 126.8, 123.3, 120.9, 111.3, 110.0, 108.3, 100.0, 65.9, 53.7, 46.4, 13.5.

Results

Pharmacokinetic analysis

The mean MM-433593 plasma concentrations resulting from intravenous and oral administration to cynomolgus monkeys are plotted over time in Figures 1 and 2, respectively. Following an intravenous dose of 1 mg/kg, the mean extrapolated initial plasma concentrations (C_0) for males and females were 2270 and 2470 ng/mL, respectively. The mean apparent volumes of the central compartment (V_c) were similar in both genders, 0.454 (males) and 0.411 L/kg (females). Exposure to MM-433593 was similar between genders. The average (±SD) area under the curve (AUC_{inf}) was 2180 ± 470 ng h/mL in males and 1760 ± 581 ng h/mL in females. The average volumes of distribution estimated for steady state (Vd_{ss}) and the terminal elimination phase (Vd_z) were large, and greater in females (8.38 and 26.0 L/kg, respectively) than in males (4.52 and 11.2 L/kg, respectively). The elimination phase half-life ($t_{1/2}$) averaged 27 h in females

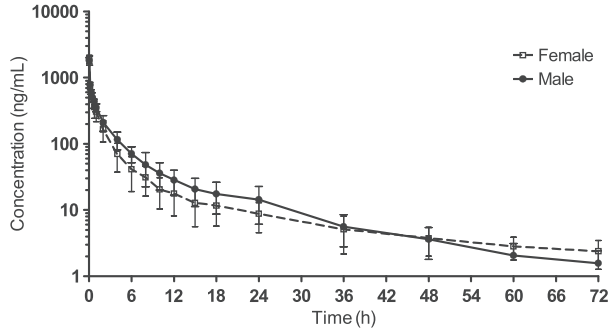

Figure 1. MM-433593 concentration-time profiles (mean ± SD) Following a 1 mg/kg intravenous administration in female and male cynomolgus monkeys.

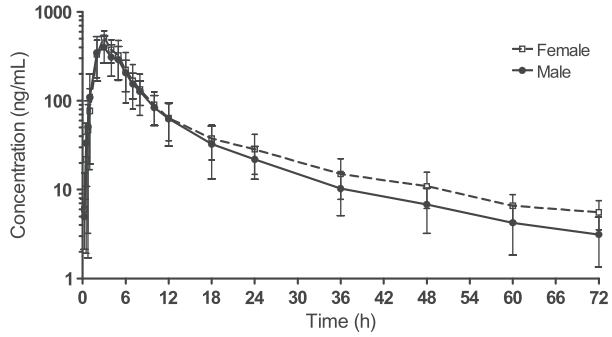

Figure 2. MM-433593 concentration-time profiles (mean ± SD) Following a 10 mg/kg oral administration in female and male cynomolgus monkeys.

and 16 h in males, and the mean residence time (MRT_{iv}) was 13.5 h in females and 9.6 h in males. The average (±SD) systemic clearance rates (CL_s) were low: 8.0 ± 1.8 mL/min/kg (males) and 10.7 ± 4.9 mL/min/kg (females).

Following oral administration, systemic exposure to MM-433593 was similar between genders. The maximum plasma concentration (C_{max}) of MM-433593 was 489 ng/mL in males and 545 ng/mL in females, and the T_{max} was observed at an average of 3.2 h in males and 3.5 h in females. The mean (± SD) AUC_{inf} was 3110 ± 619 ng h/mL and 3660 ± 1110 ng h/mL in males and females, respectively. The oral mean residence time (MRT_{po}) and apparent terminal phase half-life were slightly lower in males than females (13 h and 17 h in males versus 17 h and 20 h in females). The average observed oral clearance (CL/F) was similar between genders (55.3 mL/min/kg in males and 49.1 mL/min/kg in females). Estimates of absolute oral bioavailability (%F) ranged from 11 to 18% (14.3% mean) in males and 14 to 31% (20.8% mean) in females, with a combined average of 18% in cynomolgus monkeys. The individual and mean pharmacokinetic parameters are summarized in Table 2 and 3.

Synthesis of metabolite standards

The synthesis of metabolites M5 and M9, as outlined by Scheme 1, was achieved by starting with commercially available 5-bromo-2-methyl-1H-indole. The synthesis of 1-(4-chlorobenzyl)-3-(2-(2-methoxypyridin-4-ylamino)-2-oxoacetyl)-2-methyl-1H-indole-5-carboxylic acid M9 was achieved starting from 5-cyano-2-methyl-1H-indole A (Agarwal et al. 1993) as outlined in Scheme 1. Alkylation of indole A with 1-chloro-4-(chloromethyl)benzene followed by microwave-mediated base hydrolysis afforded carboxylic acid B, leading to divergent synthetic paths for key metabolites M5 and M9. Esterification of B was achieved using trimethylsilyldizaomethane. Subsequent treatment of this intermediate with oxalyl chloride, followed by trapping of the resulting ketoacid chloride intermediate with 2-methoxypyridine-4-amine afforded the corresponding ketoamide. Saponification of the methyl ester furnished the desired carboxylic acid metabolite M9. Reduction of carboxylic acid B with borane–tetrahydrofuran complex furnished hydroxymethyl indole C. Primary alcohol *O*-acetylation, followed by the reaction of the resultant 5-acetoxymethylindole with oxalyl chloride and subsequent trapping with 2-methoxypyridin-4-amine afforded the corresponding ketoamide. The acetate was further saponified to provide the key 5-hydroxymethylindole-metabolite M5.

Identification of metabolites

The structures of metabolites formed with monkey hepatocytes and in vivo metabolites from monkey plasma and urine were elucidated by high-resolution accurate mass measurement and product ion mass spectrometry. The presence or absence of the chlorine isotopic pattern (doublet peaks of 3:1 ratio) in the full scan mass spectrum and the characteristic fragments observed in the product ion (MS^2) spectrum of MM-433593 were used as the basis for the assignment of the metabolite structures. For key metabolites, further confirmation of the structural assignments was also made by comparison with the synthetic standards, as described below. The summary of the elemental compositions indicated by their masses are listed in Table 4. A total of 18 metabolites of MM-433593 were detected in monkey with a mass accuracy of ≤4.8 ppm from the theoretical *m/z* of predicted metabolites.

MM-433593

The ESI^+ LC/MS and ESI^+ LC/MS^2 mass spectra of MM-433593 are presented in Figure 3. The full scan mass spectrum displays an accurate mass measurement of 448.1425 Da, a 0.7 ppm deviation from the theoretical

Table 2. Intravenous MM-433593 pharmacokinetic parameters in cynomolgus monkeys.

Dose (mg/kg)	Gender	Animal number	C_0 (ng/mL)	$t_{1/2}$ (h)	AUC_{all} (ng h/mL)	AUC_{inf} (ng h/mL)	CL (mL/min/kg)	MRT_{iv} (h)	V_c (mL/kg)	Vd_{ss} (mL/kg)	Vd_z (mL/kg)
1	Male	101	1650	11.8	1570	1570	10.6	6.14	606	3900	10,800
		102	2200	24.9	2000	2090	7.96	13.3	455	6360	17,200
		103	2210	12.6	2780	2820	5.91	11.4	453	4040	6430
		104	2590	14.5	2430	2440	6.84	6.10	385	2500	8560
		105	2080	19.5	1680	1730	9.61	10.5	480	6040	16,200
		106	2910	13.7	2370	2410	6.93	10.3	344	4300	8240
		N	6	6	6	6	6	6	6	6	6
		Mean	2270	16.2	2140	2180	7.97	9.63	454	4520	11,200
		SD	434	5.1	470	470	1.80	2.92	90	1440	4460
	Female	107	2020	28.2	1640	1720	9.69	12.9	494	7510	23,600
		108	2600	36.7	1510	1640	10.2	18.0	385	11,000	32,300
		109	2490	18.1	1670	1720	9.69	9.91	401	5760	15,200
		110	2880	28.3	1890	2040	8.16	16.7	347	8190	20,000
		111	2610	18.1	2520	2610	6.39	12.9	383	4930	10,000
		112	2210	31.4	792	824	20.2	10.6	453	12,900	54,900
		N	6	6	6	6	6	6	6	6	6
		Mean	2470	26.8	1670	1760	10.7	13.5	411	8380	26,000
		SD	308	7.4	559	581	4.9	3.2	54	3050	16,100
	Male + Female	*N*	12	12	12	12	12	12	12	12	12
		Mean	2370	21.5	1900	1970	9.35	11.6	432	6450	18,600
		SD	373	8.2	550	549	3.77	3.6	74	3040	13,600

AUC, area under the curve; MRT, mean residence time.

Table 3. Oral MM-433593 pharmacokinetic parameters in cynomolgus monkeys.

Dose (mg/kg)	Gender	Animal number	T_{max} (h)	C_{max} (ng/mL)	$t_{1/2}$ (h)	AUC_{all} (ng h/mL)	AUC_{inf} (ng h/mL)	CL/F (mL/min/kg)	MRT_{po} (h)	F (%)
10	Male	113	3.0	549	18.3	2580	2630	63.4	11.4	13.4
		114	5.0	442	16.5	3870	3970	41.9	16.6	18.2
		115	4.0	529	11.2	2680	2680	62.1	7.29	12.3
		116	2.0	317	16.6	2390	2470	67.5	16.2	11.3
		117	3.0	510	27.1	3480	3680	45.2	17.4	16.9
		118	2.0	588	14.4	3180	3240	51.4	11.8	14.9
		N	6	6	6	6	6	6	6	6
		Mean	3.2	489	17.3	3030	3110	55.3	13.4	14.3
		SD	1.2	97	5.4	577	619	10.5	4.0	2.8
	Female	119	5.0	616	15.8	5320	5470	30.5	15.7	31.1
		120	3.0	541	15.7	2370	2410	69.3	11.3	13.7
		121	3.0	459	30.3	2470	2690	62.1	20.7	15.3
		122	4.0	409	19.9	3190	3390	49.1	19.7	19.3
		123	3.0	589	19.4	3960	4150	40.1	17.9	23.6
		124	3.0	654	19.7	3660	3830	43.5	14.9	21.8
		N	6	6	6	6	6	6	6	6
		Mean	3.50	545	20.1	3490	3660	49.1	16.7	20.8
		SD	0.84	95	5.4	1090	1110	14.4	3.5	6.3
	Male + Female	N	12	12	12	12	12	12	12	12
		Mean	3.3	517	18.7	3260	3390	52.2	15.1	17.5
		SD	1.0	96	5.3	869	902	12.4	3.9	5.8

AUC, area under the curve; MRT, mean residence time.

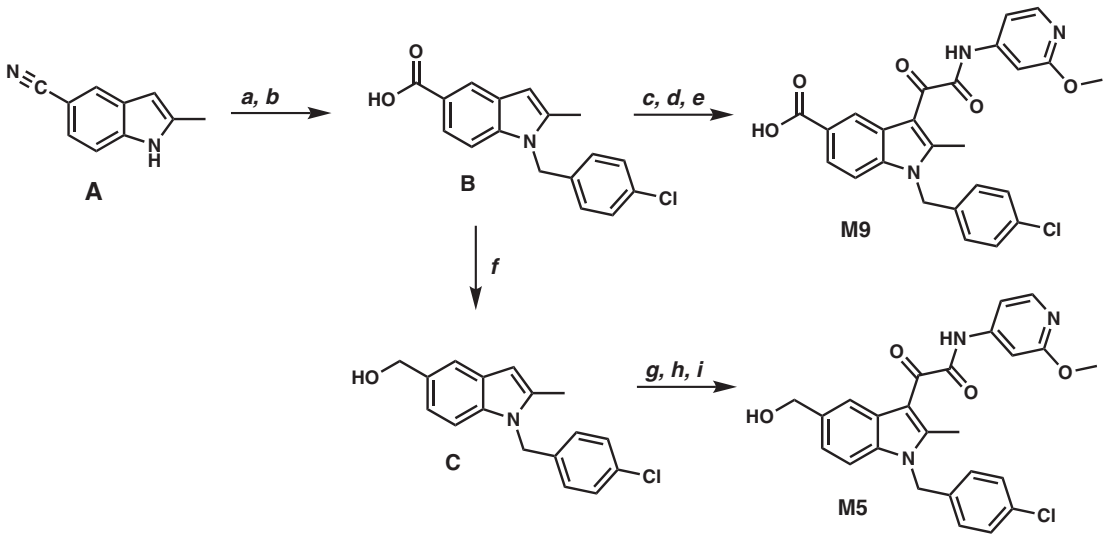

Scheme 1. Synthesis of metabolite (M5 and M9) standards. Intermediate A was prepared from 5-bromo-2-methyl-indole in 49% yield using the procedure of Agarwal et al. (1993). Reagents and conditions: (A) KOH, 1-chloro-4-(chloromethyl)benzene, DMSO, 80%; (B) KOH, EtOH, 170°C, microwave heating, 58%; (C) TMSCH2N2, Et2O/MeOH, 96%; (D) oxalyl chloride, CH2Cl2, then 2-methoxypyridin-4-amine, triethylamine, 56%; (E) NaOH, THF/H2O, 43%; (F) Borane-THF, 0°C, 79%; (G) Ac2O, triethylamine, 4-dimethylaminopyridine, 93%; (H) oxalyl chloride, CH2Cl2, then 2-methoxypyridin-4-amine, triethylamine, 67%; (I) NaOH, THF/ H2O, 75%.

Table 4. Mass spectra data and proposed structures of MM-433593 metabolites in monkey urine, plasma, and hepatocytes.

Metabolites	$[M + H]^{+1}$ Da	$\Delta m/z$ ppm	MS^2 and MS^3 product ions[2]	Description of metabolites	Samples
M1	324.1344	0.3	MS^2: 151	*N*-dealkylation	H, P
M2	434.1250	3.7	MS^2: 406, 296, 270, 137	*O*-demethylation	H, P, U
M3	310.1175	3.5	MS^2: 172, 146, 137	*N*-dealkylation and *O*-demethylation	H, P, U
M4	340.1287	1.5	MS^2: 322, 278, 151	*N*-dealkylation and aliphatic hydroxylation	H, P, U
M5	464.1355	3.7	MS^2: 446, 286, 151	Aliphatic hydroxylation	H, P, U
M6	464.1352	4.3	MS^2: 446, 339, 270, 167	Aromatic hydroxylation	P, U
M7	354.1077	2.0	MS^2: 202, 151	*N*-dealkylation, aliphatic hydroxylation and oxidation	H, P, U
M8	480.1308	2.7	MS^2: 462, 434, 167	Aliphatic and aromatic hydroxylations	H, U
M9	478.1149	3.1	MS^2: 434, 326, 151	Aliphatic hydroxylation and oxidation	H, P, U
M10	494.1096	3.4	MS^2: 167	Aromatic hydroxylation and aliphatic hydroxylation and oxidation	U
M11	420.0840	4.8	MS^2: 340, 151	*N*-dealkylation and aliphatic hydroxylation and sulfation	P, U
M12	516.1595	1.5	MS^2: 488, 340, 151	*N*-dealkylation and aliphatic hydroxylation and glucuronidation	H, P, U
M13	640.1681	1.7	MS^2: 464, 446, 294	Aliphatic hydroxylation and glucuronidation	H, P, U
M14	544.0922	3.3	MS^2: 464, 446MS^3: 286, 151	Aliphatic hydroxylation and sulfation	H, U
M15	656.1630	1.8	MS^2: 638, 480, 462, 310	Aromatic hydroxylation and aliphatic hydroxylation and glucuronidation	U
M16	530.1386	3.6	MS^2: 512, 494, 354, 336, 151	*N*-dealkylation and aliphatic hydroxylation and oxidation and glucuronidation	P, U
M17	654.1473	1.8	MS^2: 636, 618, 478, 460, 326	Aliphatic hydroxylation and oxidation and glucuronidation	H, P, U
M18	609.1563	1.0	MS^2: 446 MS^3: 418, 402, 296	Aliphatic hydroxylation and GSH conjugation	H, U

P, plasma; U, urine; H, hepatocytes.

[1]Measured accurate mass of protonated molecule $[M + H]^+$.

[2]Major or significant product ions.

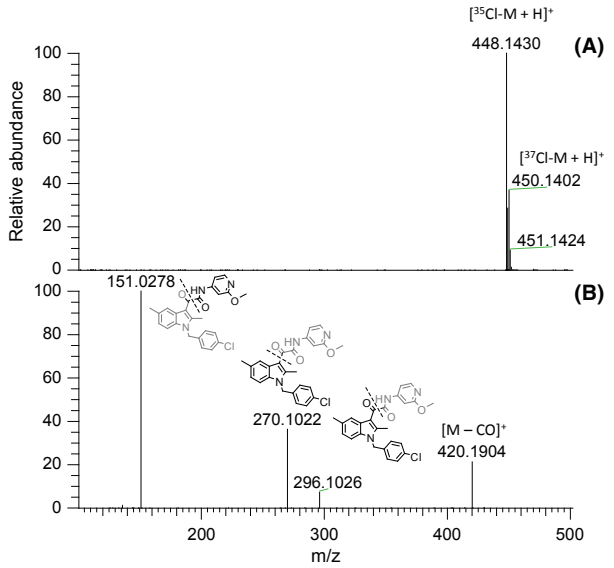

Figure 3. +ESI LC/MS (A) and MS^2 at *m/z* 448 (B) mass spectrum of MM-433593 showing the chlorine isotopic pattern and the proposed fragments.

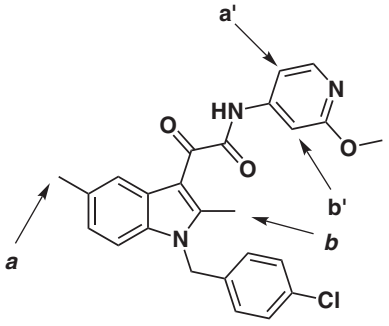

Figure 4. Structure of MM-433593. Arrows shows possible sites of hydroxylation.

value of the protonated molecule $[M+H]^+$ (Table 1) with the characteristic pattern of chlorine isotope (^{37}Cl), a doublet peak of 3:1 ratio. The product ion mass spectrum of MM-433593 displayed several characteristic fragments corresponding to the structures shown in Figure 3.

M1

The LC/MS spectrum of M1 displayed a protonated measured mass of 324.1344 Da, a 0.3 ppm deviation from the mass predicted for an *N*-dealkylated-MM-433593 metabolite (Table 4). The absence of the chlorine isotope pattern was clearly evident in the full scan mass spectrum of M1, confirming the loss of the chlorobenzyl moiety from the parent. The product ion mass spectrum showed only a prominent ion at *m/z* 151, characteristic of the 2-methoxy-4-amido-pyridine portion of the metabolite.

M2

The LC/MS spectrum of M2 displayed a measured mass of 434.1270 Da, a 0.9 ppm deviation from the mass predicted for an MM-433593 metabolite with one less methyl group (Table 4). Further confirmation of the identity was provided by the LC/MS^2 spectrum which displayed a distinctive fragment at *m/z* 137, due to 2-hydroxy-4-amido-pyridine, indicating the loss of a methyl group from the pyridine portion of MM-433593.

M3

The LC/MS spectrum of M3 displayed a measured mass of 310.1175 Da, a 3.5 ppm deviation from the mass predicted for an *N*-dealkylated-, *O*-demethylated-MM-433593 metabolite (Table 4). The absence of the chlorine isotope pattern was clearly indicative of the loss of the chlorobenzyl moiety in M3. The product ion mass spectrum displayed a characteristic fragment at *m/z* 137, due to 2-hydroxy-4-amido-pyridine and implying the loss of a methyl group from the pyridine portion of the molecule. This metabolite can be readily formed by *N*-dealkylation and *O*-demethylation of MM-433593 in either order.

M4

The LC/MS spectrum of M4 displayed a measured mass of 340.1287 Da, a 1.5 ppm deviation from the mass predicted for a product of *N*-dealkylated-hydroxy-MM-433593 metabolite (Table 4). The absence of a chlorine isotopic pattern was evident in the full scan mass spectrum of M4. The product ion mass spectrum displayed a fragment at *m/z* 151, characteristic of the 2-methoxy-4-amido-pyridine portion of the metabolite, indicating that the hydroxylation did not occur on the pyridine ring. Fragments were also observed at *m/z* 322 and *m/z* 278, resulting from loss of water and collective losses of both CO_2 and water from the protonated molecule, respectively. Since the water is more readily lost from alcohols than phenols, it is a reasonable assumption that the hydroxylation took place on one of the two methyls on the indole ring. Moreover, since *methyl a* is sterically more accessible than *methyl b*, (Fig. 4) the hydroxylation is more likely to occur at methyl *a*. Although the alternative modification site cannot be ruled out, the metabolite is most likely formed by *N*-dealkylation and aliphatic hydroxylation of MM-433593.

M5

The LC/MS spectrum of M5 displayed a measured mass of 464.1355 Da, a 3.7 ppm deviation from the mass pre-

dicted for an oxidized-MM-433593 metabolite (Table 4). The full scan mass spectrum of M5 showed the characteristic chlorine isotopic pattern of 3:1 ratio of *m/z* 464 to *m/z* 466. The product ion mass spectrum displayed the distinct fragment at *m/z* 151 due to 2-methoxy-4-amido-pyridine moiety, indicating that the oxidation did not take place on the pyridine portion of the metabolite. This was further supported by the fragment at *m/z* 286, which revealed that oxidation on the indole moiety of the molecule had occurred. As discussed for M4, hydroxylation of sterically more accessible *methyl a* of the indole ring (Fig. 4) appears to be more favorable than *methyl b*. This was further confirmed by comparison of HPLC retention times and LC/MS fragmentation patterns with that of the M5 synthetic standard. The two compounds displayed identical HPLC retention times and product ion fragmentation patterns.

M6

The LC/MS spectrum of M6 displayed a measured mass of 464.1352 Da, a 4.3 ppm deviation from the mass predicted for an oxidized-MM-433593 metabolite (Table 4). The full scan spectrum of M6 displayed the characteristic of a chlorine isotope pattern. The product ion mass spectrum of this metabolite was quite different from that of hydroxymethyl-433593 (M5). It displayed a unique fragment ion at *m/z* 167, 16 mass units higher than the corresponding fragment seen for the 2-methoxy-4-amido-pyridine portion (*m/z* 151) in M5 and MM-433593 mass spectrum. This clearly indicated that for this metabolite hydroxylation took place on the pyridine portion of the MM-433593. Since both the methoxy and the amido substituents on the pyridine ring are *ortho*/*para* directing and the pyridine ring itself is *meta* directing, there are two possible positions on the pyridine ring for hydroxylation (*a*′ and *b*′ as shown in Fig. 4). Although the alternative modification site cannot be ruled out, the electrophilic hydroxylation most likely occurred at the more accessible *a*' position.

M7

The LC/MS spectrum of M7 displayed a measured mass of 354.1077 Da, a 0.6 ppm deviation from the mass predicted for a *N*-dealkylated-5-carboxylic acid-MM-433593 metabolite (Table 4). As with M4, the absence of the chlorine isotopic pattern was clearly evident in the mass spectrum of M7. The product ion mass spectrum of this metabolite displayed only one intense fragment peak at *m/z* 151, characteristic of the 2-methoxy-4-amido-pyridine portion of the metabolite.

M8

The LC/MS spectrum of M8 displayed a measured mass of 480.1308 Da, a 2.7 ppm deviation from the mass predicted for dihydroxy-MM-433593 metabolite (Table 4). The product ion mass spectrum displayed a distinct fragment peak at *m/z* 167 indicative of hydroxylation on the pyridine ring of MM-433593. Fragments were also observed at *m/z* 462 and *m/z* 434, which resulted from loss of water and collective losses of both water and a carbonyl group, respectively, from the protonated molecule. M8 was only found in urine and not circulating in plasma and was identified as hydroxymethyl-hydroxypyridyl-MM-433593. This metabolite can be formed by oxidation of M5 on the pyridine ring.

M9

The LC/MS spectrum of M9 displayed a measured mass of 478.1149 Da, a 3.1 ppm deviation from the mass predicted for an oxidized-MM-433593 metabolite (Table 4). The full scan mass spectrum of M9 showed the characteristic isotopic pattern of chlorine and the product ion mass spectrum displayed the distinct 2-methoxy-4-amido-pyridine fragment peak at *m/z* 151 indicating that the oxidation did not take place on the pyridine ring. The fragment at *m/z* 450 was due to the loss of carbonyl (CO, 28 Da) and the fragment at *m/z* 326 revealed the aliphatic oxidation of a methyl to carboxylic acid functionality. This was further confirmed by comparison of HPLC retention times and LC/MS fragmentation patterns with the M9 synthetic standard.

M10

The LC/MS spectrum of M10 displayed a measured mass of 494.1096 Da, a 3.4 ppm deviation from the mass predicted for an oxidized MM-433593 metabolite (Table 4). The full scan mass spectrum of M10 showed the distinctive chlorine isotopic pattern. The product ion mass spectrum displayed an intense fragment peak at *m/z* 167, characteristic of the 2-methoxy-4-amido-hydroxypyridine, indicating hydroxylation on the pyridine ring. This metabolite was only found in urine.

M11

The LC/MS spectrum of M11 displayed a measured mass of 420.0840 Da, a 4.8 ppm deviation from the mass predicted for the sulfate conjugate of M4 (Table 4). The full scan mass spectrum showed the protonated molecule

$[M+H]^+$ at *m/z* 420 without the chlorine isotopic pattern. The product ion mass spectrum of this metabolite displayed an intense peak at *m/z* 340, resulting from the loss of sulfate (80 Da) from the protonated molecule $[M + H]^+$, and a fragment peak at *m/z* 151 characteristic of the 2-methoxy-4-amido-pyridine.

M12

The LC/MS spectrum of M12 displayed a measured mass of 516.1596 Da, a 1.5 ppm deviation from the mass predicted for the glucuronide conjugate of M4 (Table 4). The product ion mass spectrum of M12 displayed two intense fragments; one at *m/z* 340, due to the loss of glucuronide (176 Da) from the protonated molecule $[M + H]^+$, and one at *m/z* 151 characteristic of the 2-methoxy-4-amido-pyridine moiety.

M13

The LC/MS spectrum of M13 displayed a measured mass of 640.1681 Da, a 1.7 ppm deviation from the mass predicted for the glucuronide conjugate of M5 (Table 4). The product ion mass spectrum of M13 displayed characteristic fragments at *m/z* 464 that resulted from the loss of glucuronide (176 Da), and at *m/z* 446 that resulted from collective losses of both glucuronide and a molecule of water (194 Da) from the protonated molecule $[M + H]^+$.

M14

The LC/MS spectrum of M14 displayed a measured mass of 544.0922 Da, a 3.3 ppm deviation from the accurate mass predicted for the sulfate conjugate of M5 (Table 4). The full scan mass spectrum showed the protonated molecule $[M+H]^+$ at *m/z* 544 with the characteristic chlorine isotopic pattern. The product ion mass spectrum displayed two characteristic fragments; *m/z* 464 consistent with loss of sulfate (80 Da), and *m/z* 446 resulting from the losses of both sulfate and a water (98 Da) from the protonated molecule. This metabolite was only found in urine and not circulating in plasma.

M15

The LC/MS spectrum of M15 displayed a measured mass of 656.1630 Da, a 1.8 ppm deviation from the mass predicted for the glucuronide conjugate of M8 (Table 4). The full scan mass spectrum showed the protonated molecule $[M+H]^+$ at *m/z* 656 with the chlorine isotopic pattern. The product ion mass spectrum of M15 displayed several characteristic fragments; at *m/z* 638, due to the loss water, and at *m/z* 480 and *m/z* 462, due to the loss of glucuronide and collective losses of both glucuronide and a water, respectively, from the protonated molecule $[M + H]^+$. This metabolite was only found in urine.

M16

The LC/MS spectrum of metabolite M16 displayed a measured mass of 530.1386 Da, a 3.6 ppm deviation from the mass predicted for the glucuronide conjugate of M7 (Table 4). The product ion mass spectrum of M16 displayed fragments at *m/z* 512, due to the loss of water; *m/z* 354, due to the loss of a glucuronide conjugate (176 Da), and at *m/z* 336, due to the combined losses of both glucuronide and a molecule of water (194 Da) from the $[M + H]^+$ peak.

M17

The LC/MS spectrum of M17 displayed a measured mass of 654.1473 Da, a 1.8 ppm deviation from the mass predicted for the product of M9 conjugation with glucuronide (Table 4). The product ion mass spectrum of M17 displayed fragments at *m/z* 636 and *m/z* 618, due to the loss of one and two molecules of water, respectively, from the $[M + H]^+$ peak. Fragments were also observed at *m/z* 478 and

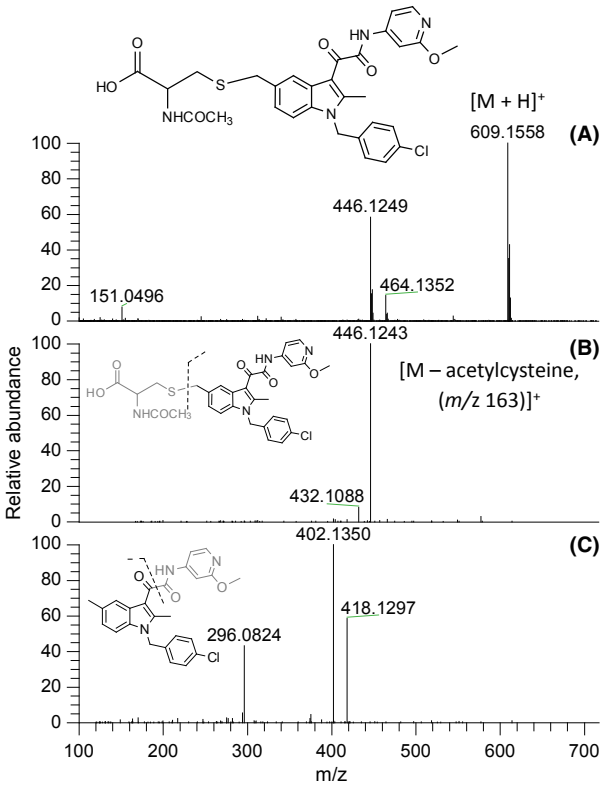

Figure 5. +ESI LC/MS of protonated M18 (A), MS^2 at *m/z* 609 (B), and MS^3 at *m/z* 446 (C) mass spectrum of Metabolite M18.

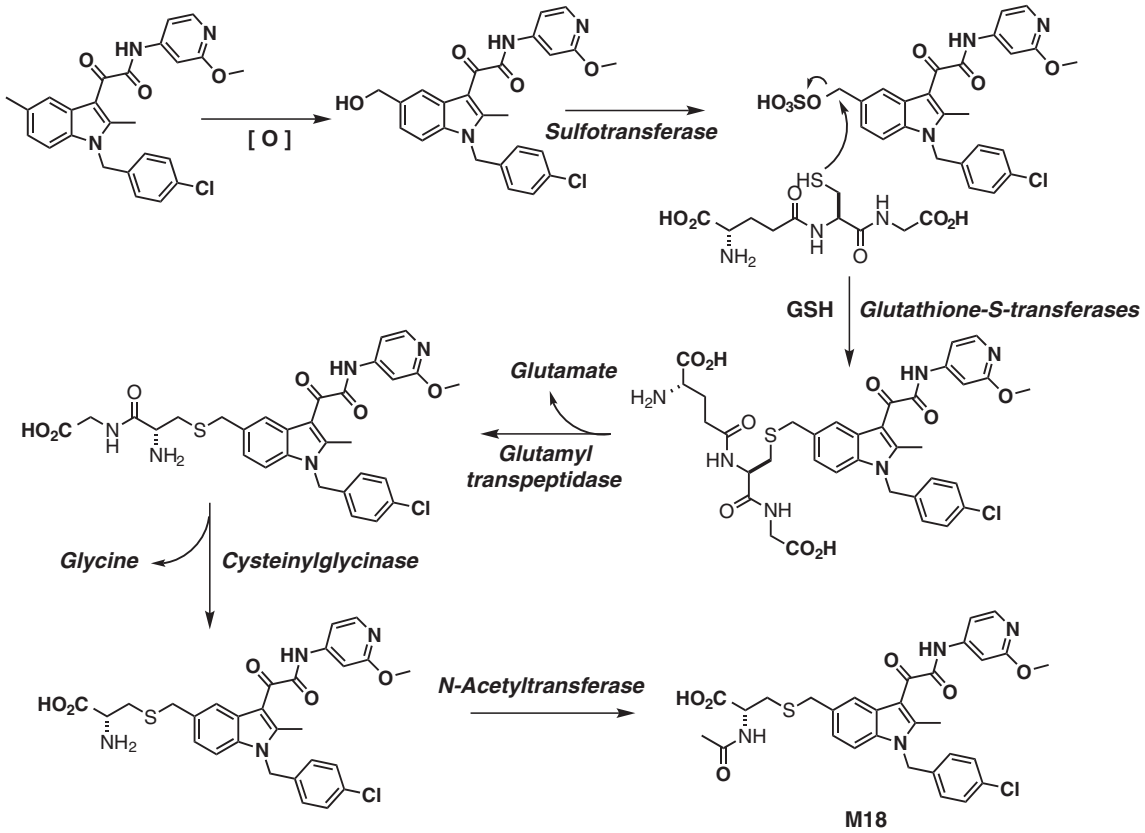

Scheme 2. Proposed pathway for the formation of MM-433593-*N*-acetylcysteine conjugate (M18).

m/z 460, due to the loss of glucuronide and combined losses of both glucuronide and a molecule of water, respectively, from the protonated molecule $[M + H]^+$.

M18

The LC/MS spectrum of M18 displayed a measured mass of 609.1563 Da, <1 ppm deviation from the mass predicted for the *N*-acetylcysteine conjugate of MM-433593 (Table 4). A 161 Da higher mass than MM-433593 for this metabolite along with the even-numbered molecular weight observed for M18 was indicative of the conjugation of MM-433593 with *N*-acetylcysteine. This was supported further by the product ion mass spectrum (MS^2) which displayed a prominent fragment at *m/z* 446, resulting from the loss of protonated-*N*-acetylcysteine (*m/z* 163), from the protonated molecule peak (Fig. 5). Further fragmentation of the *m/z* 446 ion (MS^3) produced fragments at *m/z* 418 and *m/z* 402, resulting from loss of CO and CO_2, respectively, and at *m/z* 296, corresponding to the characteristic structural fragment shown in Figure 5. This metabolite was only found in urine and not circulating in plasma and was identified as MM-433593-*N*-acetylcysteine. Glutathione conjugation generally occurs on substrates containing an electrophilic carbon attached to a leaving group such as a sulfate or a halide. Therefore, it was proposed that M18 was formed from M14. As shown in Scheme 2 glutathione conjugation with M14 could be catalyzed by *glutathione-S-transferase*. This putative MM-433593-glutathione conjugate could then undergo further metabolism by loss of glutamine, catalyzed by *glutamyl transpeptidase*, followed by the loss of glycine, catalyzed by *cysteinyl glycinase*, to form the MM-433593-cysteine conjugate. The MM-433593-cysteine conjugate could then be acetylated by *N-acetyltransferase* to produce MM-433593-*N*-acetylcysteine as the final product. The metabolite structure as well as the proposed biotransformation pathway for the formation of M18 from MM-433593 are shown in Scheme 2.

Discussion

To investigate the fate of MM-433593 in cynomolgus monkeys, the nonrodent species used in toxicology studies, the pharmacokinetics was evaluated and metabolites were identified in hepatocyte incubations as well as in plasma and urine samples collected after 5 days of dosing at 1000 mg/kg.

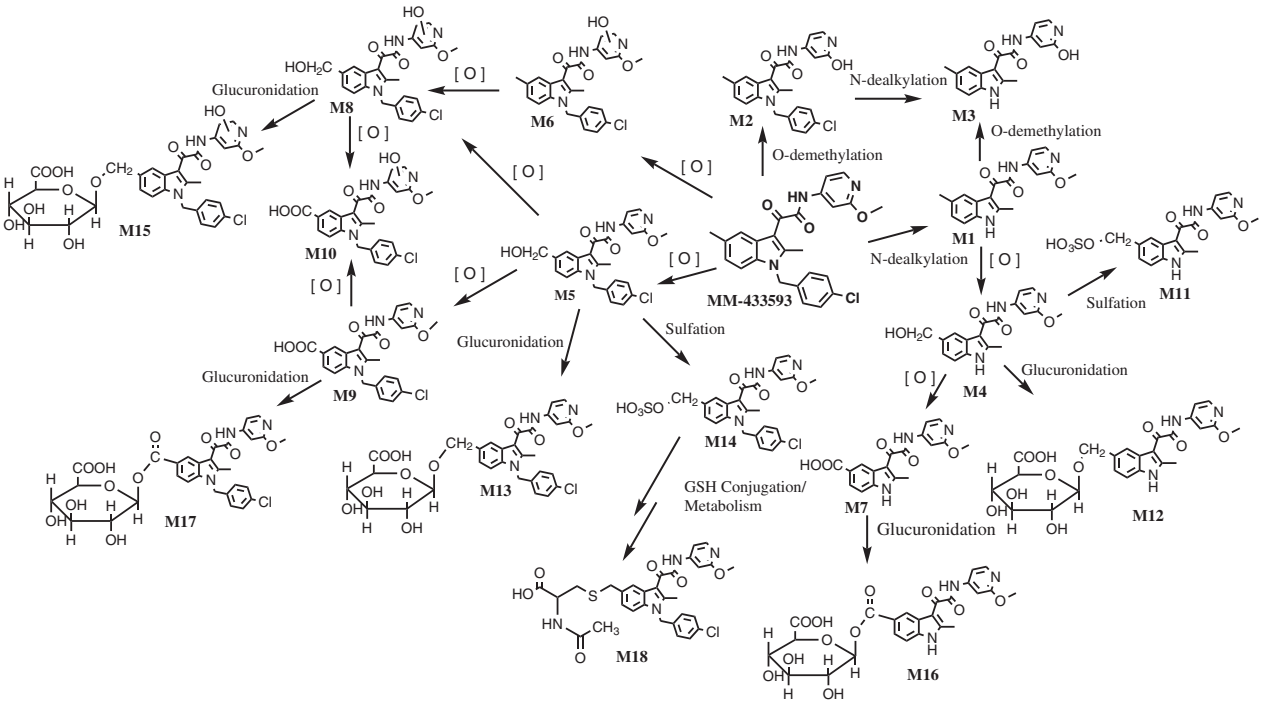

Scheme 3. Proposed pathway for the metabolism of MM-433593 in cynomolgus monkeys.

The pharmacokinetics of MM-433593 was similar in male and female monkeys. Intravenous administration of MM-433593 produced a rapid distribution phase and a slower elimination phase. The volume of distribution was large, indicating a preferential partitioning into tissues, and the systemic clearance was low. The maximum MM-433593 plasma concentration was reached ~3 h after an oral dose, and the estimated bioavailability was moderate (18%).

MM-433593 underwent phase I and phase II biotransformations and produced at least 18 metabolites in male and female monkeys; 13 circulating metabolites were identified in plasma and 17 were identified in urine. With the exception of M1, all of the metabolites identified in plasma were also present in the urine and there were no apparent gender differences. In vitro metabolism with monkey hepatocytes produced 13 metabolites, all of which were also found in vivo, either in plasma or urine or both. The aromatic hydroxylation metabolites were found in the urine but were often absent from plasma samples and hepatocyte incubations.

The proposed pathway for metabolism of MM-433593 in cynomolgus monkey is presented in Scheme 3. The major biotransformation pathway of MM-433593 involves oxidation of the methyl group at the five position of the indole ring to produce M5. This was confirmed by LC/MS comparison with the authentic synthesized standard. Further oxidation of M5 resulted in formation of the carboxylic acid metabolite (M9) which in turn underwent glucuronide conjugation to produce metabolite M17. In addition, M5 formed conjugates with glucuronides (M13), sulfate (M14), and glutathione (M18). A plausible pathway for the formation of M18 was proposed via further reaction of M14, as presented in Scheme 2.

MM-433593 is broadly metabolized involving several types of oxidative and conjugation pathways. All in vitro metabolites produced by monkey hepatocytes were also found in vivo and the predicted metabolic pathways were confirmed in the plasma and urine of monkeys. This strong in vitro/in vivo correlation provides further support for anticipating the potential human metabolites of MM-433593 using human hepatocytes in advance of clinical studies.

Acknowledgements

The authors would like to thank Sean Toole for formatting the figures to the journal's specifications.

Disclosure

None declared.

References

Agarwal A, Jalluri RK, Blanton CD, Taylor EW (1993). A new synthesis of the potent 5-HT1 receptor ligand, 5-carboxy-amidotryptamine (5-CT). Synth Commun 23: 1101–1110.

Ahn K, Johnson DS, Mileni M, Beidler D, Long JZ, McKinney MK, et al. (2009). Discovery and characterization of a highly selective FAAH inhibitor that reduces inflammatory pain. Chem Biol 16: 411–420.

Blankman JL, Cravatt BF (2013). Chemical probes of endocannabinoid metabolism. Pharmacol Rev 65: 849–871.

Calignano A, La Rana G, Giuffrida A, Piomelli D (1998). Control of pain initiation by endogenous cannabinoids. Nature 394: 277–281.

Cravatt BF, Lichtman A (2003). Fatty acid amide hydrolase: an emerging therapeutic target in the endocannabinoid system. Curr Opin Chem Biol 7: 469–475.

Cravatt BF, Giang DK, Mayfield SP, Boger DL, Lerner RA, Gilula NB (1996). Molecular characterization of an enzyme that degrades neuromodulatory fatty-acid amides. Nature 384: 83–87.

Cravatt BF, Demarest K, Patricelli MP, Bracey MH, Giang DK, Martin BR, et al. (2001). Supersensitivity to anandamide and enhanced endogenous cannabinoid signaling in mice lacking fatty acid amide hydrolase. Proc Natl Acad Sci USA 98: 9371–9376.

Cravatt BF, Saghatelian A, Hawkins EG, Clement AB, Bracey MH, Lichtman AH (2004). Functional disassociation of the central and peripheral fatty acid amide signaling systems. Proc Natl Acad Sci USA 101: 10821–10826.

Goparaju SK, Ueda N, Yamaguchi H, Yamamoto S (1998). Anandamide amidohydrolase reacting with 2-arachidonoylglycerol, another cannabinoid ligand. FEBS Lett 422: 69–73.

Jaggar SI, Hasnie FS, Sellaturay S, Rice AS (1998). The anti-hyperalgesic actions of the cannabinoid anandamide and the putative CB2 receptor agonist palmitoylethanolamide in visceral and somatic inflammatory pain. Pain 76: 189–199.

Maccarrone M (2006). Fatty acid amide hydrolase: a potential target for next generationtherapeutics. Curr Pharm Des 12: 759–772.

Piomelli D (2003). The molecular logic of endocannabinoid signalling. Nat Rev Neurosci 4: 873–884.

Schlosburg JE, Kinsey SG, Lichtman AH (2009). Targeting fatty acid amide hydrolase (FAAH) to treat pain and inflammation. AAPS J 11: 39–44.

Wei BQ, Mikkelsen TS, McKinney MK, Lander ES, Cravatt BF (2006). A second fatty acid amide hydrolase with variable distribution among placental mammals. J Biol Chem 281: 36569–36578.